Universal relations of local order parameters for partially synchronized oscillators

Oleh E. Omel'chenko,[1] Michael Sebek,[2] and István Z. Kiss[2]

[1]*Weierstrass Institute, Mohrenstrasse 39, 10117 Berlin, Germany*
[2]*Department of Chemistry, Saint Louis University, 3501 Laclede Avenue, St. Louis, Missouri 63103, USA*

Interactions among discrete oscillatory units (e.g., cells) can result in partially synchronized states when some of the units exhibit phase locking and others phase slipping. Such states are typically characterized by a global order parameter that expresses the extent of synchrony in the system. Here we show that such states carry data-rich information of the system behavior, and a local order parameter analysis reveals universal relations through a semicircle representation. The universal relations are derived from thermodynamic limit analysis of a globally coupled Kuramoto-type phase oscillator model. The relations are confirmed with the partially synchronized states in numerical simulations with a model of circadian cells and in laboratory experiments with chemical oscillators. The application of the theory allows direct approximation of coupling strength, the natural frequency of oscillations, and the phase lag parameter without extensive nonlinear fits as well as a self-consistency check for presence of network interactions and higher harmonic components in the phase model.

I. INTRODUCTION

Synchronization of rhythmic processes is an important phenomenon [1–5] that underlies the functioning of many essential physiological processes, e.g., in cardiac pacemaker cells [6] and circadian clock neurons [7]. The interpretation of data often relies on the Kuramoto-Sakaguchi model [8] type of phase equations, which formulate the instantaneous frequencies (time derivative of the phases) as a function of the phase difference between the oscillations [9]. In fact, this model is relevant to any globally (all-to-all) coupled oscillator system provided the oscillators are in the regime close to the onset of oscillations through a Hopf bifurcation and the interaction between them is weak. Other applications where validity of this model was rigorously justified include Josephson junctions arrays [10,11] and electrical circuit oscillators [12–14].

The oscillatory units (e.g., cells with periodic gene expressions) are often partially synchronized: The oscillations are neither fully synchronized, nor fully desynchronized, but in a state in between that provides a balance for generation of strong rhythm and ability to adapt to external change. The partially synchronized states can be described through extensive experiments with changing the coupling strengths, plotting the order parameter as a function of the coupling strength, and comparing the experimental results to the theoretical predictions [15–19]. The type of behavior depends on the distribution of natural frequencies, coupling strength, and the oscillation sheer (phase shift in the coupling that can slow down or speed up weakly coupled oscillators without phase locking) [20]. Present theoretical approaches focus on solving the asymptotic behavior of the Kuramoto-Sakaguchi equation, typically showing the order parameters as a function of coupling strength assuming that the frequency distribution and the phase shift parameter are known [21,22].

Experimental data (in particular in biological systems) can be often collected only at a given coupling strength, and *a priori* very little is known about the phase shift parameter or the exact natural frequencies of oscillators. Therefore, a question arises whether some universal relations exist for the evolution of the phases in terms of the Kuramoto-Sakaguchi equation, that could be compared to the experimental data at the given coupling strength.

In this paper, we show the existence of the universal properties of the partially synchronized states of the Kuramoto-Sakaguchi equation in the thermodynamic limit. A synchronization analysis is developed, which relies on the behavior of the local order parameter. The use of a semicircle representation is tested in numerical calculations with finite-size phase models and with a model of circadian gene expressions, as well as in experiments with chemical oscillators.

II. KURAMOTO-SAKAGUCHI MODEL

The Kuramoto-Sakaguchi model [8]

$$\frac{d\theta_k}{dt} = \omega_k - \frac{K}{N} \sum_{j=1}^{N} \sin(\theta_k - \theta_j + \alpha), \quad k = 1, \ldots, N, \quad (1)$$

describes dynamics of N globally coupled phase oscillators $\theta_k \in \mathbb{R}$ mod 2π with the natural frequencies ω_k drawn randomly from a specific distribution $g(\omega)$. Given a distribution $g(\omega)$ and a phase-lag parameter $\alpha \in (-\pi/2, \pi/2)$ and varying coupling strength K from zero to large positive values one usually observes synchronization transition scenario [23,24] shown schematically in Fig. 1. The synchronization is characterized with the Kuramoto order parameter

$$r(t) = \frac{1}{N} \sum_{k=1}^{N} e^{i\theta_k(t)}, \quad (2)$$

which measures the synchrony between oscillators such that $|r(t)| = 1$ and $|r(t)| \approx 0$ stand for the perfectly synchronous state and for disordered phase configurations, respectively. If coupling K is smaller than a certain critical value K_c, then the
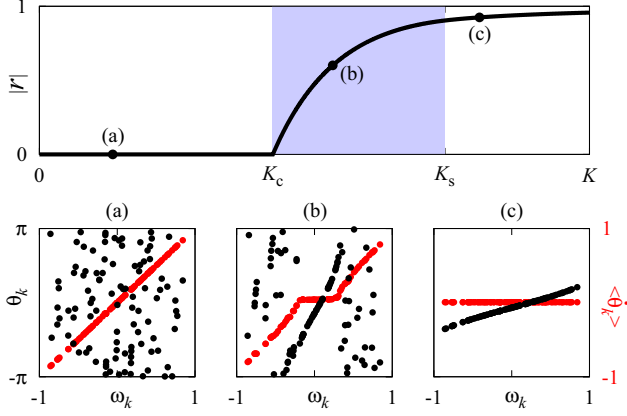
FIG. 1. Synchronization transition in the Kuramoto-Sakaguchi model (1) with large number of oscillators N. Incoherence (a), partial synchrony (b), and phase-locked state (c) are observed for $K < K_c$, $K_c < K < K_s$, and $K > K_s$, respectively, where K_c and K_s are threshold values depending on $g(\omega)$ and α. Additional panels show phase snapshots θ_k and time-averaged phase velocities $\langle \dot{\theta}_k \rangle$ typical for these states.

asynchronous (incoherent) state, Fig. 1(a), is stable. For larger coupling strengths one observes the onset of partial synchrony, Fig. 1(b), with $|r(t)|$ growing with the increase of K. Finally, when K exceeds another critical value K_s all oscillators get phase locked, Fig. 1(c).

Modulus $|r(t)|$ usually exhibits finite-size fluctuations, and therefore in practice one replaces it with the mean order parameter

$$R = \langle |r(t)| \rangle, \tag{3}$$

where the angle brackets $\langle \cdot \rangle$ denote time average. Moreover, a detailed representation of stationary regimes in the supercritical region, i.e., for $K \geqslant K_c$, can be obtained if one records the effective frequencies

$$\Omega_k = \left\langle \frac{d\theta_k}{dt} \right\rangle = \lim_{T \to \infty} \frac{\theta_k(T) - \theta_k(0)}{T}. \tag{4}$$

In this paper, for each oscillator we also define a complex quantity characterizing its mutual entrainment to the mean field, the *local order parameter*,

$$\zeta_k = \left\langle -i e^{i\theta_k(t)} \frac{\overline{r}(t)}{|r(t)|} \right\rangle \in \mathbb{C}, \tag{5}$$

where $\overline{r}(t)$ denotes the complex conjugate of $r(t)$. The oscillator with $|\zeta_k| = 1$ is synchronized (or phase locked) with respect to the Kuramoto order parameter $r(t)$, while the oscillator with $|\zeta_k| < 1$ is desynchronized and drifts with respect to it. Note that motivation for definition (5) originates from formula (A15) in Appendix A.

It turns out that in many cases the triplet $(R, \{\Omega_k\}, \{\zeta_k\})$ constitutes a unique signature of the state developed by the system (1). In Sec. III we show that the elements of this triplet satisfy some universal relations.

The universal relations allow a simple approximation of parameters of the system (1) from partially synchronized states (Secs. IV A and IV B). Moreover, these relations allow to demonstrate the nonuniqueness of parameter reconstruction

for phase-locked states (Sec. IV C) and identify the Kuramoto-Sakaguchi model among other Kuramoto-type models (Sec. IV D). In Sec. V we show two examples illustrating the application of universal relations for primary treatment of the data in circadian oscillators and experiments with electrochemical oscillators. Some concluding remarks are given in Sec. VI.

Two Appendices at the end of the paper summarize the details of the thermodynamic limit analysis for the Kuramoto-Sakaguchi model (Appendix A) and describe the experimental setup for electrochemical oscillators (Appendix B).

III. UNIVERSAL RELATIONS

In the limit $N \to \infty$ the state of the phase oscillators $\{\theta_k(t)\}$ can be described by a probability density function $\rho(\theta, \omega, t)$ such that $\rho(\theta, \omega, t) \, d\omega \, d\theta$ determines the probability to find oscillator with $(\omega_k, \theta_k(t)) \in [\omega, \omega + d\omega] \times [\theta, \theta + d\theta]$ at the time t. The mean-field structure of Eq. (1) allows us to write a nonlinear hyperbolic integrodifferential equation, the so-called *continuity equation*, describing the evolution of $\rho(\theta, \omega, t)$. This equation can be analyzed using the method suggested by Ott and Antonsen in Refs. [25,26]. In particular, it can be shown, see Appendix A, that all stationary partially synchronized states of Eq. (1) are represented by a two-parametric family of periodic solutions of the continuity equation [50]. Explicit form of these solutions and numerically observed ergodicity of partially synchronized states result in the following identities:

$$R = p/K, \tag{6}$$

$$\zeta_k = h(s_k) e^{-i\alpha}, \tag{7}$$

$$\Omega_k = \Omega + p Q(s_k), \tag{8}$$

where

$$s_k = \frac{\omega_k - \Omega}{p}, \tag{9}$$

and $(\Omega, p) \in \mathbb{R} \times (0, \infty)$ is a pair of numbers parameterizing the manifold of partially synchronized states. A remarkable feature of formulas (7) and (8) is that their right-hand sides are expressed via the two universal functions

$$h(s) = \begin{cases} (1 - \sqrt{1 - s^{-2}})s & \text{for} \quad |s| > 1, \\ s - i\sqrt{1 - s^2} & \text{for} \quad |s| \leqslant 1, \end{cases} \tag{10}$$

and

$$Q(s) = \begin{cases} s\sqrt{1 - s^{-2}} & \text{for} \quad |s| > 1, \\ 0 & \text{for} \quad |s| \leqslant 1, \end{cases} \tag{11}$$

which are independent of the particular choice of natural frequencies ω_k and other system parameters K and α, therefore we call these formulas *universal relations*. In Sec. III A we show that although formulas (6)–(8) are justified for the limit $N \to \infty$ only, they remain a good approximation for large but fixed sizes N, too.

Accuracy of universal relations

In order to test formulas (6)–(8) in the finite-N case we performed a series of numerical simulations of model (1) with
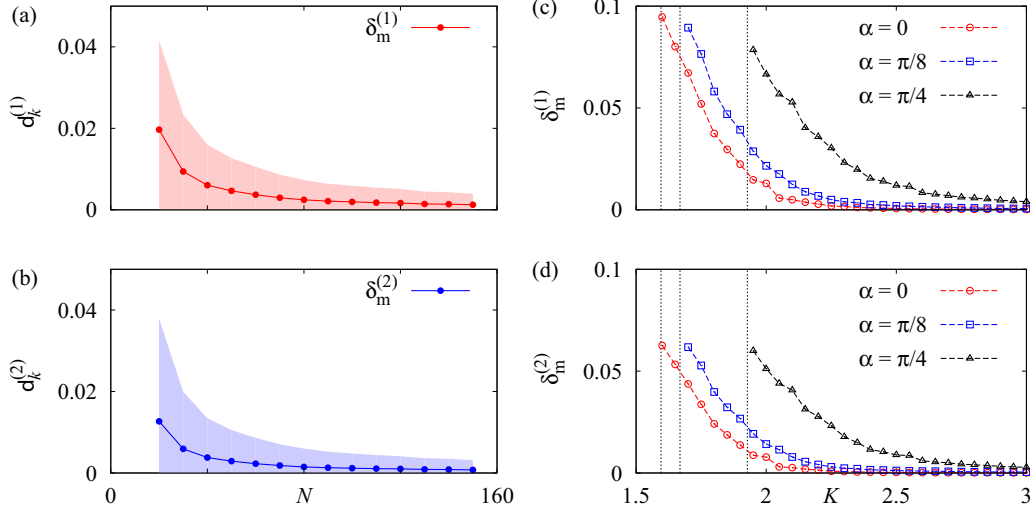
FIG. 2. Accuracy of universal relations (6)–(8) for the Kuramoto-Sakaguchi model (1). Panels (a) and (b): Distribution of discrepancies $d_k^{(1)}$ and $d_k^{(2)}$ for different system sizes N. Solid lines show mean values $\delta_m^{(1)}$ and $\delta_m^{(2)}$. Shaded regions show the intervals $[0, \delta_m^{(n)} + \sigma_m^{(n)}]$ containing most of $d_k^{(n)}$. Panels (c) and (d): Mean discrepancies $\delta_m^{(1)}$ and $\delta_m^{(2)}$ for different values of K and α. Vertical dotted lines show the onset of synchrony K_c for chosen values of α.

natural frequencies ω_k drawn randomly from the Gaussian distribution

$$G(\omega) = \frac{1}{\sqrt{2\pi}} e^{-\omega^2/2}.$$

For fixed system size N and fixed parameters K and α we generated 1000 realizations of the natural frequencies ω_k. For each realization we integrated system (1) using the Runge-Kutta scheme with the constant time step $dt = 0.02$. Starting from random initial conditions and discarding a transient of the length 1000 time units, we used next $T = 1000$ time units to calculate the observables R, ζ_k, and Ω_k. More precisely, we used formulas (3)–(5) where time averages $\langle \ldots \rangle$ were replaced with their finite-time analogs

$$\langle \ldots \rangle_T = \frac{1}{T} \int_0^T (\ldots)\, dt. \tag{12}$$

Mean-field velocity (or rotational velocity of order parameter) was computed from the formula

$$\Omega = \frac{\mathrm{Arg}\, r(T) - \mathrm{Arg}\, r(0)}{T},$$

where $\mathrm{Arg}\, r(t)$ denotes the continuously varying argument of the order parameter $r(t)$.

Given K, ω_k, R, and Ω we computed p and s_k from (6) and (9). Inserting them into formulas (7) and (8) and dividing the latter by $p = KR$ we obtained two dimensionless expressions

$$d_k^{(1)} = \left| \zeta_k - h\left(\frac{\omega_k - \Omega}{KR} \right) e^{-i\alpha} \right|, \tag{13}$$

$$d_k^{(2)} = \left| \frac{\Omega_k - \Omega}{KR} - Q\left(\frac{\omega_k - \Omega}{KR} \right) \right|, \tag{14}$$

measuring the discrepancy in each of formulas (7) and (8). The distribution of discrepancies $d_k^{(1)}$ and $d_k^{(2)}$ was charcterized by

the mean values

$$\delta^{(n)} = \frac{1}{N} \sum_{k=1}^{N} d_k^{(n)}, \quad n = 1, 2,$$

and the variances

$$\sigma^{(n)} = \sqrt{\frac{1}{N} \sum_{k=1}^{N} \left(d_k^{(n)} - \delta^{(n)} \right)^2}, \quad n = 1, 2.$$

Averaging them over 1000 realizations of the natural frequencies ω_k we obtained mean values $\delta_m^{(n)}$ and $\sigma_m^{(n)}$.

Figures 2(a) and 2(b) show that formulas (6)–(8) are satisfied with good accuracy already for moderate system sizes N. The accuracy is better than 10% already for $N \geqslant 30$ oscillators and the mean discrepancy decreases inversely proportional to the system size N.

Figures 2(c) and 2(d) explain how the accuracy of formulas (6)–(8) depends on the values of the coupling strength K and the phase lag α. In general, we observe the following tendency. The accuracy is very good for all values (K, α) where partially synchronized states exist, except of the values close to the onset of partial synchronization. In this case interaction between oscillators is very weak and cannot be identified with satisfactory resolution. Taking into account the scaling behavior shown in Figs. 2(a) and 2(b), one may expect that for increasing system size the region of low accuracy of formulas (6)–(8) becomes smaller and shrinks for $N \to \infty$.

IV. APPLICATION OF UNIVERSAL RELATIONS

Now we show some applications of universal relations (6)–(8). In Sec. IV A we formulate a mathematical algorithm allowing to approximate all parameters of the Kuramoto-Sakaguchi model (1) from the triplet $(R, \{\Omega_k\}, \{\zeta_k\})$ corresponding to a partially synchronized state. The accuracy of this approach is analyzed in Sec. IV B. Next, in Sec. IV C we show that for phase-locked states the parameter reconstruction problem
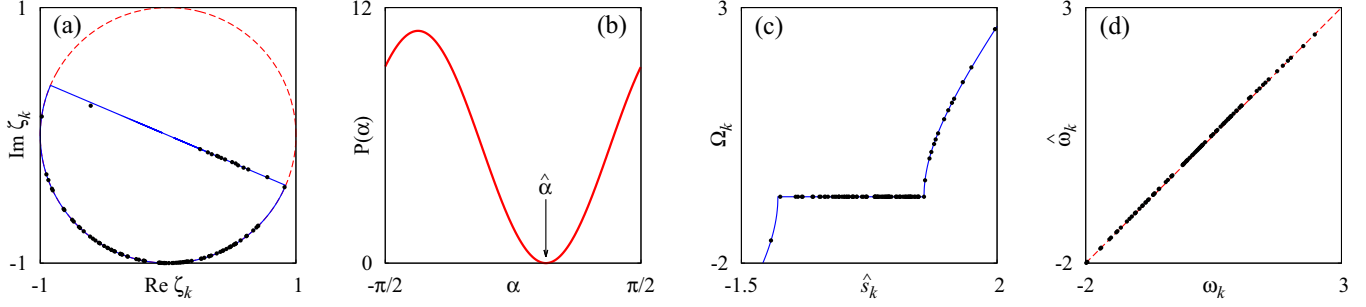
FIG. 3. Data representation and parameter approximation for numerical simulation data from model (1). (a) Computed values of ζ_k (dots) and their semicircle fit (solid curve). (b) Approximated phase lag $\hat{\alpha}$ is the minimum of the function $P(\alpha)$, see formula (16). (c) The best fit (solid curve) of the dependence between Ω_k and $\hat{s}_k$ (dots). (d) Approximated $\hat{\omega}_k$ vs. actual ω_k natural frequencies. Parameter approximation quality: (a) $C_1 = 4.3 \times 10^{-5}$ and (c) $1 - C_2 = 1.2 \times 10^{-5}$.

has infinitely many solutions constituting a two-dimensional manifold. Finally, in Sec. IV D we show how universal relations (6)–(8) can be used to discriminate between the Kuramoto-Sakaguchi model and more complicated Kuramoto-type models with inhomogeneous coupling topology and nonsinusoidal phase interaction functions.

A. Parameter approximation

Suppose that we observe a stationary partially synchronized state in system (1) and measure the instantaneous phases $\theta_k(t)$ of all oscillators over a time interval of length T. For sufficiently large T time averages $\langle \ldots \rangle$ in formulas (3)–(5) are well approximated by their finite-time analogs $\langle \ldots \rangle_T$, see (12). Thus, we can calculate the mean order parameter R, the effective frequencies Ω_k, and the local order parameters ζ_k of the oscillators. For a partially synchronized state we must have $0 < R < 1$. Moreover, the effective frequencies Ω_k cannot be completely locked, i.e., at least some of them must be different.

For the local order parameters, by definition we have $|\zeta_k| \leqslant 1$. Moreover, for partially synchronized states, formula (7) implies that points ζ_k are located at the boundary of a unit semicircle, which is the image of $h(s)e^{-i\alpha}$ for $s \in \mathbb{R}$, see Fig. 3(a). This fact can be used to calculate the phase lag α from the plot of local order parameters ζ_k as follows.

Function $h(s)$ defined by formula (10) satisfies the equation

$$s = \frac{h^2(s) + 1}{2h(s)} \in \mathbb{R}, \quad (15)$$

therefore, to fit the relation (7) we seek a phase lag parameter α that minimizes the function

$$P(\alpha) = \sum_{k=1}^{N} \left[\text{Im}\left(\frac{\zeta_k^2 e^{2i\alpha} + 1}{2\zeta_k e^{i\alpha}} \right) \right]^2 = 2B - 2\text{Re}(Ae^{2i\alpha}), \quad (16)$$

where

$$A = \sum_{k=1}^{N} \frac{(|\zeta_k|^2 - 1)^2 \zeta_k^2}{16|\zeta_k|^4}, \quad B = \sum_{k=1}^{N} \frac{(|\zeta_k|^2 - 1)^2}{16|\zeta_k|^2}.$$

Simple calculations demonstrate that for $|A| \neq 0$ function $P(\alpha)$ has a unique minimum $\hat{\alpha} \in (-\pi/2, \pi/2)$ given by

$$\hat{\alpha} = -\frac{1}{2} \arg A, \quad (17)$$

see Fig. 3(b). For infinitely large systems equations (7) are exact, therefore formula (17) yields true value of phase lag α in Eq. (1), while for finite-size systems we may expect that $\hat{\alpha}$ is a good approximation of α. The latter will be verified in Sec. IV B.

Next, using $\hat{\alpha}$ we calculate the approximated rescaled natural frequencies

$$\hat{s}_k = \text{Re}\left(\frac{\zeta_k^2 e^{2i\hat{\alpha}} + 1}{2\zeta_k e^{i\hat{\alpha}}} \right). \quad (18)$$

Because of (8) the points in the $(\hat{s}_k, \Omega_k)$ graph should follow $\Omega_k = \Omega + pQ(\hat{s}_k)$, where p is the frequency scaling factor and Ω is the frequency of the order parameter $r(t)$, see Fig. 3(c). Since for partially synchronized states we have $|\hat{s}_k| > 1$ at least for some fraction of indexes k, this relationship allows us to formulate a linear fitting procedure

$$\sum_{k=1}^{N} (\Omega_k - \Omega - pQ(\hat{s}_k))^2 = \min$$

determining the parameters p and Ω. Its solution can be written explicitly,

$$\hat{p} = \frac{N\Sigma_{\Omega Q} - \Sigma_\Omega \Sigma_Q}{N\Sigma_{QQ} - \Sigma_Q^2}, \quad \hat{\Omega} = \frac{1}{N}\Sigma_\Omega - \frac{\hat{p}}{N}\Sigma_Q,$$

where

$$\Sigma_\Omega = \sum_{k=1}^{N} \Omega_k, \quad \Sigma_{\Omega Q} = \sum_{k=1}^{N} \Omega_k Q(\hat{s}_k),$$

$$\Sigma_Q = \sum_{k=1}^{N} Q(\hat{s}_k), \quad \Sigma_{QQ} = \sum_{k=1}^{N} Q(\hat{s}_k)^2.$$

To quantify the correlation between measured data $\theta_k(t)$ and formulas (6)–(8) one can use two fitting quality coefficients:

(a) The quality of the semicircle fit is described by the ratio

$$C_1 = \frac{\min P(\alpha)}{\max P(\alpha)} = \frac{B - |A|}{B + |A|}, \quad (19)$$

which measures how pronounced is the minimum of function $P(\alpha)$. Ideally C_1 must be close to zero. Large C_1 corresponds to poor correlation between the input data R, ζ_k, Ω_k, and formulas (6)–(8).

(b) The quality of the linear fit is determined by the corresponding correlation coefficient

$$C_2 = \frac{N \Sigma_{\Omega Q} - \Sigma_\Omega \Sigma_Q}{\sqrt{N \Sigma_{QQ} - \Sigma_Q^2} \sqrt{N \Sigma_{\Omega\Omega} - \Sigma_\Omega^2}}, \qquad (20)$$

where $\Sigma_{\Omega\Omega}$ is defined by analogy with Σ_{QQ}. $|C_2|$ values close to 1 represent good fit.

If the semicircle fit and the linear fit confirm that measured data agree with formulas (6)–(8), then all parameters of this model can be calculated: The phase shift can be obtained using Eq. (17), and the effective coupling strength and the natural frequencies can be calculated as follows:

$$\hat{K} = \hat{p}/R \quad \text{and} \quad \hat{\omega}_k = \hat{\Omega} + \hat{p}\hat{s}_k. \qquad (21)$$

B. Parameter approximation accuracy

The accuracy of the parameter approximation algorithm from Sec. IV A was tested by applying it to surrogate data from numerical simulations of model (1). We used the same protocol as in Sec. III A. Namely, for fixed system size N and fixed parameters K and α we generated 1000 realizations of the Gaussian distributed natural frequencies ω_k. For each realization we integrated system (1) starting from random initial conditions. Discarding a transient of the length 1000 time units, we used next $T = 1000$ time units to calculate the observables R, ζ_k, and Ω_k from the formulas (3)–(5) where time averages $\langle \dots \rangle$ were replaced with their finite-time analogs $\langle \dots \rangle_T$. The approximation error of the modified formulas (3)–(5) was computed by

$$E = \max_{\tau \in [T/2, T]} |\langle \dots \rangle_\tau - \langle \dots \rangle_T|.$$

[For the chosen averaging time $T = 1000$ this error was much smaller than the corresponding mean discrepancies $\delta_m^{(1,2)}$ of universal relations (6)–(8).]

Computed values R, ζ_k and Ω_k were processed using the parameter approximation algorithm from Sec. IV A. For example, Fig. 3 shows how the algorithm works for model (1) with $N = 100$, $K = 2.5$, and $\alpha = \pi/8$.

For each realization we calculated two fitting quality coefficients C_1 and C_2 defined by (19) and (20) as well as the reconstruction errors

$$E_\omega = \frac{1}{N} \sum_{k=1}^{N} |\hat{\omega}_k - \omega_k|, \quad E_K = \frac{|\hat{K} - K|}{K}, \quad E_\alpha = \frac{|\hat{\alpha} - \alpha|}{\pi/4},$$

where K, α, ω_k are input parameters and $\hat{K}, \hat{\alpha}, \hat{\omega}_k$ are their approximated values. A mean error estimate was calculated by averaging the errors over 1000 realizations. Note that because of the finite system size N, for a given natural frequency realization there exists a critical coupling strength K_s such that for $K \geqslant K_s$ system (1) has a global phase-locked state attractor. If in our simulations we encountered such a realization, then we discarded it and generated a new one until we obtained a system (1) exhibiting a partially synchronized state.

Figure 4 shows the dependence of the parameter approximation accuracy on the system size N, while Fig. 5 explains how

FIG. 4. Parameter approximation accuracy for the Kuramoto-Sakaguchi model (1) with Gaussian frequency distribution $G(\omega)$ and different sizes N. (a) Reconstruction errors of natural frequencies E_ω, coupling strength E_K, and phase lag E_α. (b) Fitting quality coefficients C_1 and C_2.
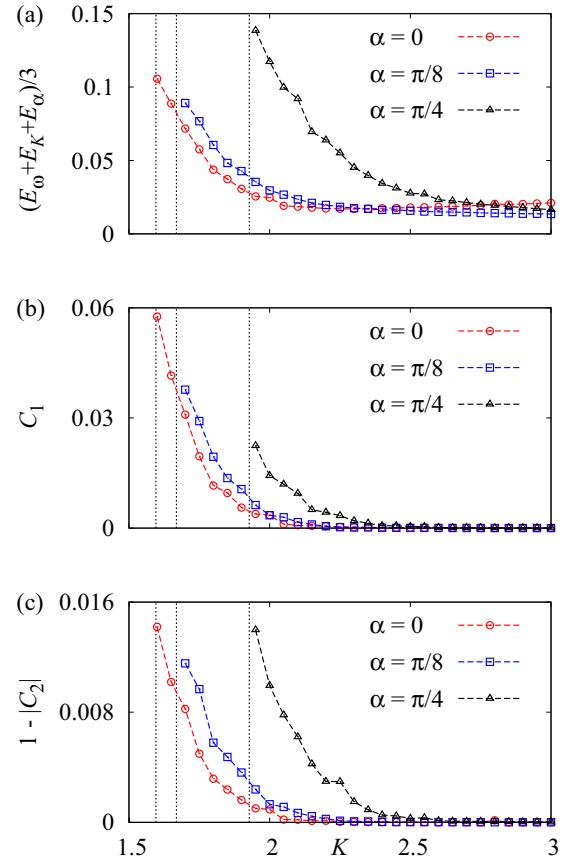
FIG. 5. Parameter approximation accuracy for the Kuramoto-Sakaguchi model (1) with Gaussian frequency distribution $G(\omega)$ and different values of K and α. Notations E_ω, E_K, E_α, C_1, and C_2 are the same as in Fig. 4. Vertical dotted lines show the onset of synchrony K_c for chosen values of α.
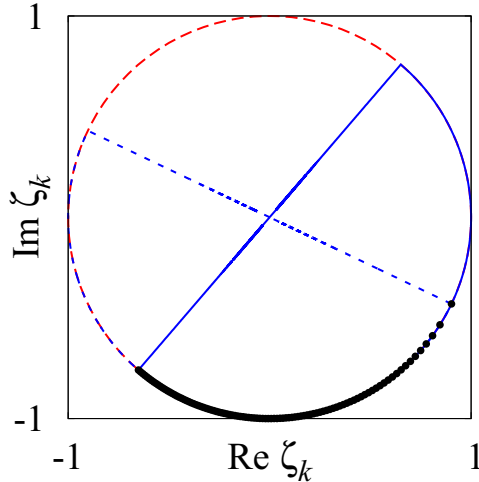
FIG. 6. Local order parameters ζ_k (dots) of a phase-locked state in the Kuramoto-Sakaguchi model (1) with uniformly distributed natural frequencies $\omega_k = -1 + 2k/(N-1)$. Parameters: $N = 100$, $K = 1.7$, and $\alpha = \pi/8$. The tilts of the dotted and solid semicircles determine phase lags $\hat{\alpha}_{\min}$ and $\hat{\alpha}_{\max}$.

this accuracy depends on the values of the coupling strength K and the phase lag α. Comparing these results with Fig. 2 we see that the accuracy of the parameter approximation algorithm varies similarly to the accuracy of universal relations (6)–(8). In particular, it decreases inversely proportional to the system size N and remains nearly constant for all values (K, α) where partially synchronized states exist, except of the values close to the onset of partial synchronization. Moreover, the fitting quality coefficients C_1 and C_2 shown in Figs. 4(b), 5(b), and 5(c) confirm that formulas (6)–(8) indeed are satisfied with good accuracy in all tests.

C. Parameter approximation for phase-locked states

For large coupling strengths K system (1) exhibits phase-locked states characterized by identical effective frequencies Ω_k. In this case all oscillators are entrained to the mean field, and therefore $|\zeta_k| = 1$ for all $k = 1, \ldots, N$. Thermodynamic limit analysis shows that formulas (6)–(8) remain valid for phase-locked states, too. However, the reconstruction algorithm from Sec. IV A does not give a unique solution for system parameters ω_k, K, and α. Indeed, if we look at the graph of local order parameters ζ_k of a phase-locked state, see Fig. 6, we find that there exist two angles $\hat{\alpha}_{\min}, \hat{\alpha}_{\max} \in (-\pi/2, \pi/2)$ such that for every $\alpha \in [\hat{\alpha}_{\min}, \hat{\alpha}_{\max}]$ all points ζ_k lie on the semicircle $\{h(s)e^{-i\alpha} : s \in \mathbb{R}\}$. In this case, we cannot use formula (8) to determine the parameter p, because for $|\zeta_k| = 1$ formula (18) yields $|\hat{s}_k| \leqslant 1$ and hence $Q(\hat{s}_k) = 0$. However, if we assume $\hat{\Omega} = \Omega_k$ (recall that all Ω_k are identical), then for arbitrary choice of

$$(\hat{\alpha}, \hat{p}) \in [\hat{\alpha}_{\min}, \hat{\alpha}_{\max}] \times (0, \infty)$$

formulas (21) determine parameters $\hat{K}$ and $\hat{\omega}_k$ of the system (1) consistent with the observed triplet $(R, \{\Omega_k\}, \{\zeta_k\})$. Thus, the parameter approximation problem has a two-parametric set of solutions.

D. Identification of the Kuramoto-Sakaguchi model

Partially synchronized states similar to those shown in Fig. 1(b) can be found not only in the Kuramoto-Sakaguchi model (1) but also in more complicated Kuramoto-type models with nonglobal coupling or phase interaction which is not purely sinusoidal. To identify such situations and distinguish them from the case of a simpler Kuramoto-Sakaguchi model, one can use additional mathematical tests based on the universal relations (A19) and (A20) from Appendix A.

Nonglobal coupling. The Kuramoto-Sakaguchi model (1) is a special case of the model

$$\frac{d\theta_k}{dt} = \omega_k - \frac{K_k}{N} \sum_{j=1}^{N} \sin(\theta_k - \theta_j + \alpha), \quad k = 1, \ldots, N, \quad (22)$$

with nonidentical coupling strengths K_k. Suppose that in system (22) we observe a partially synchronized state with a triplet $(R, \{\Omega_k\}, \{\zeta_k\})$. Using the reconstruction algorithm we can erroneously identify this state as a state in the Kuramoto-Skaguchi model and reconstruct its coupling strength $\hat{K}$, phase lag $\hat{\alpha}$, and natural frequencies $\hat{\omega}_k$. To avoid the misinterpretation, we have to calculate N parameters

$$\hat{K}_k = \frac{\hat{\omega}_k - \Omega_k}{R \, \mathrm{Re}(\zeta_k e^{i\hat{\alpha}})}. \quad (23)$$

According to the formula (A20) from Appendix A, for the Kuramoto-Sakaguchi model (1) all $\hat{K}_k$ must be identical. In contrast, if coupling topology between oscillators is nonglobal, then this property is violated. The L^∞-variance is sufficient to characterize this effect:

$$\Delta K = \max_k \hat{K}_k - \min_k \hat{K}_k.$$

To illustrate the proposed test we consider the model (22) with coupling strengths K_k evenly distributed in the interval $[K(1 - \varepsilon), K(1 + \varepsilon)]$ with $\varepsilon > 0$, i.e.,

$$K_k = K\left[1 - \varepsilon + \frac{2\varepsilon(k-1)}{N}\right]. \quad (24)$$

For fixed ε we computed a trajectory of system (22) and processed it with the parameter approximation algorithm from Sec. IV A. Figure 7 shows the dependence of ΔK on ε for $N = 100$, $K = 2.5$, $\alpha = \pi/8$ and a particular realization of Gaussian distributed natural frequencies ω_k. As expected, the variance ΔK is negligibly small for $\varepsilon = 0$ and increases monotonously for growing ε. For $N = 100$, mean accuracy of the coupling strength reconstruction is $K E_K \approx 0.032$, see Fig. 4(a). Hence, every measurement $\Delta K > 0.032$ (above the shaded region in Fig. 7) indicates that the measured triplet $(R, \{\Omega_k\}, \{\zeta_k\})$ does not fit the Kuramoto-Sakaguchi model. This means that for chosen parameters we can reliably detect inhomogeneities exceeding 7% of K.

Nonsinusoidal phase interaction. Partially synchronized states can also be found in the Kuramoto-type models with global coupling but nonsinusoidal interaction between oscillators. For example, this can be the Kuramoto-Daido model,

$$\frac{d\theta_k}{dt} = \omega_k - \frac{K}{N} \sum_{j=1}^{N} f(\theta_k - \theta_j), \quad (25)$$
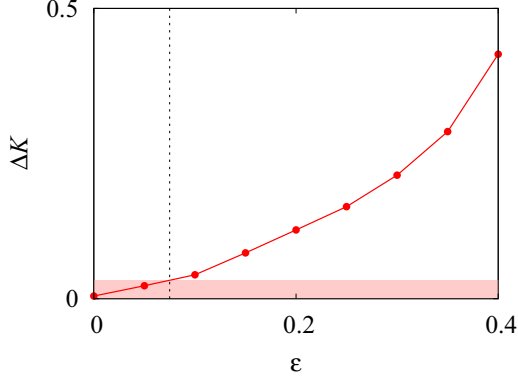
FIG. 7. Variance ΔK for the model (22) and (24) with different widths ε of the coupling strength distribution (24). Parameters: $N = 100$, $K = 2.5$, $\alpha = \pi/8$ and some realization of Gaussian distributed natural frequencies ω_k.

where

$$f(\theta) = \sin(\theta + \alpha) + \gamma \sin(2\theta). \quad (26)$$

In order to discriminate between the Kuramoto-Sakaguchi model (1) and a more complicated model (25), we can look at the local order parameters of higher orders,

$$\zeta_k^{(n)} = \left\langle (-i)^n e^{in\theta_k(t)} \frac{\overline{r}(t)^n}{|r(t)|^n} \right\rangle, \quad n = 2, 3, \ldots.$$

The Ott-Antonsen theory [25] says [see formula (A19) in Appendix A] that for purely sinusoidal phase interaction, i.e., $\gamma = 0$, all partially synchronized states lie in the manifold satisfying identities $\zeta_k^{(n)} = \zeta_k^n$, where $\zeta_k \equiv \zeta_k^{(1)}$. To detect deviations from this property we can monitor the expressions

$$\Delta_n = \max_k \left| 1 - \frac{\zeta_k^{(n)}}{\zeta_k^n} \right|, \quad n = 2, 3, \ldots.$$

Figure 8 shows the dependence of Δ_2 on γ for $N = 100$, $K = 2.5$, $\alpha = \pi/8$ and a particular realization of Gaussian distributed natural frequencies ω_k. The indicator function Δ_2 is almost vanishing for $\gamma = 0$ and is separated from zero for
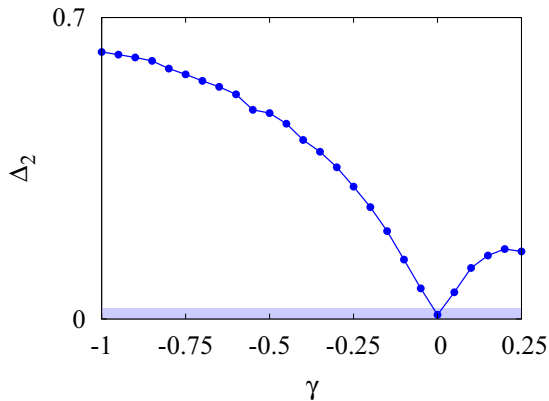
FIG. 8. Indicator function Δ_2 for the Kuramoto-Daido model (25)–(26) with $\gamma \in [-1, 0.25]$. Other parameters: $N = 100$, $K = 2.5$, $\alpha = \pi/8$ and some realization of Gaussian distributed natural frequencies ω_k.

$\gamma \neq 0$. To make this criterion preciser we take into account that the mean discrepancy $\delta_m^{(1)}$, see Sec. III A, can be considered as expected accuracy of local order parameters ζ_k. Then the accuracy of ζ_k^2 equals $2\delta_m^{(1)}$ and the accuracy of Δ_2 is likely to be $4\delta_m^{(1)}$. Now, if $\Delta_2 > 4\delta_m^{(1)}$ (shaded region in Fig. 8), then we can conclude that phase interaction function $f(\theta)$ is not purely sinusoidal but contains higher-order harmonics.

V. PRACTICAL EXAMPLES

In this section we demonstrate the application of the universal relations (6)–(8) and the reconstruction algorithm from Sec. IV A in two realistic experiments.

A. Circadian oscillators

We consider a population of $N = 100$ circadian oscillators [27]. Each oscillator is described by a three-dimensional system of ordinary differential equations (ODEs)

$$\frac{dM_k}{dt} = v_{s,k} \frac{K_I^n}{K_I^n + P_{N,k}^n} - v_{m,k} \frac{M_k}{K_m + M_k}, \quad (27)$$

$$\frac{dP_{C,k}}{dt} = k_s M_k - v_d \frac{P_{C,k}}{K_d + P_{C,k}} - k_1 P_{C,k} + k_2 P_{N,k}, \quad (28)$$

$$\frac{dP_{N,k}}{dt} = k_1 P_{C,k} - k_2 P_{N,k}, \quad (29)$$

where M_k is nuclear mRNA (e.g., *Period*), $P_{C,k}$, and $P_{N,k}$ are the cytosolic and nuclear clock protein concentrations in the kth cell, and the kinetic parameters are set to $n = 4$, $K_I = 1$ nM, $K_m = 0.5$ nM, $k_s = 0.417$ 1/h, $v_d = 1.167$ nM/h, $K_d = 0.13$ nM, $k_1 = 0.417$ nM/h, and $k_2 = 0.5$ nM/h. The inherent heterogeneities of individual cells are modelled by choosing parameters $v_{m,k}$ in Eq. (27) from a Gaussian distribution with a standard deviation of 4×10^{-3} nM/h and a mean value of 0.5 nM/h. The coupling between oscillators is global and is defined by [28]

$$v_{s,k}(t) = v_0 + \varkappa[M_{\text{av}}(t) - M_k(t)],$$

where $v_0 = 0.83$ nM/h, $\varkappa = 0.02$ 1/h and

$$M_{\text{av}}(t) = \frac{1}{100} \sum_{k=1}^{100} M_k(t).$$

Physically, the coupling increases the maximum transcription rate of a cell based on the difference between the mRNA level of the kth cell and the mean group levels through a multistep, vasoactive intestinal peptide (VIP) receptor-mediated mechanism [28].

The mRNA level of the kth cell $M_k(t)$ is used to determine the geometric phase of the corresponding oscillation,

$$\phi_k(t) = \arg[M_k(t) - \langle M_k(t) \rangle - i \dot{M}_k(t)],$$

where $\langle M_k(t) \rangle$ denotes the time average of $M_k(t)$. Then we apply formulas of the universal relations, using the geometric phases ϕ_k instead of the unknown physical phases θ_k. Figure 9(a)–9(e) shows results for a particular numerical experiment at an intermediate coupling strength that generates a partially synchronized state. The experimental data fit well the semicircle, with a tilt that corresponds to a large positive
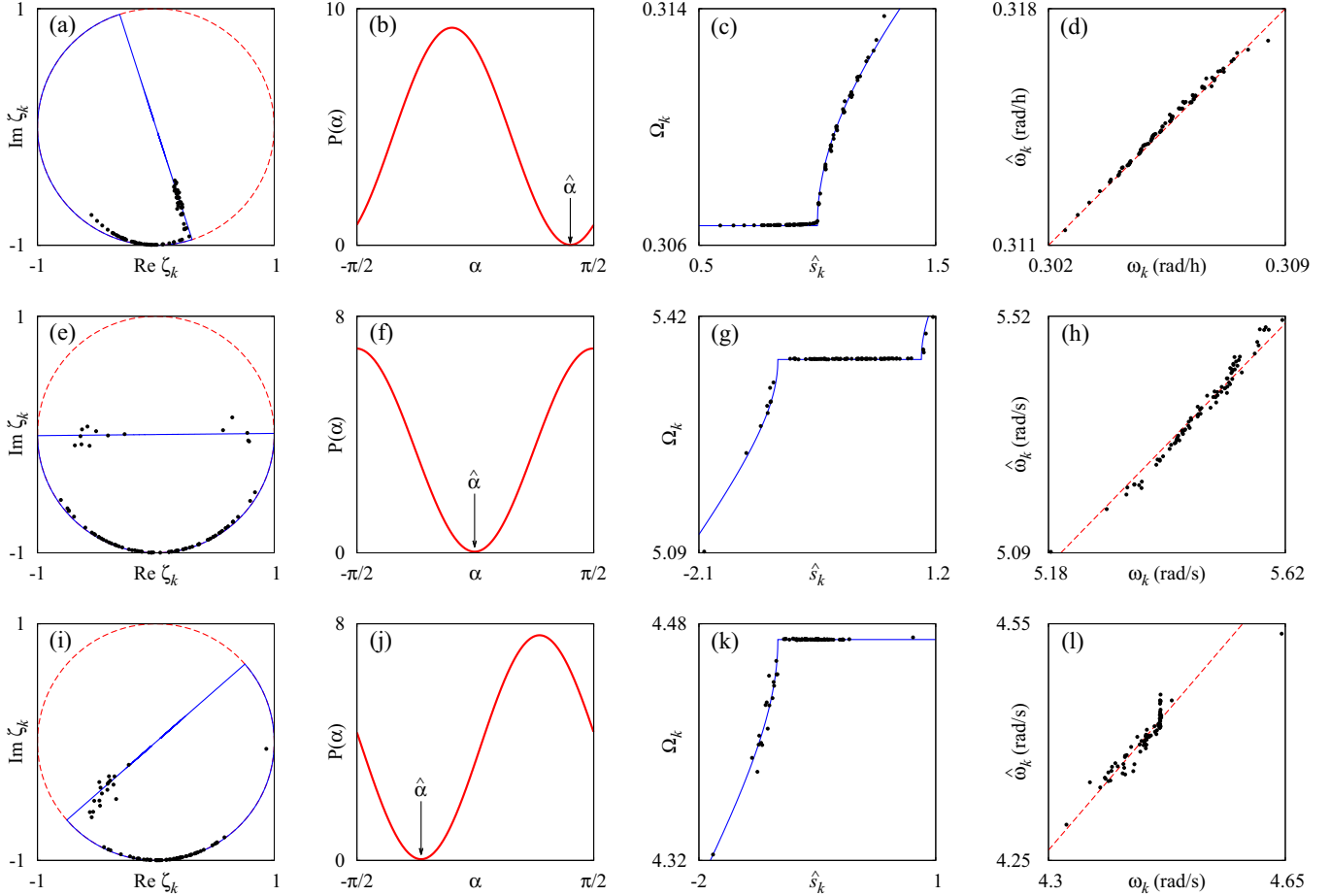
FIG. 9. Data representation and parameter approximation for numerical simulation data from a model of circadian cells [panels (a)–(d)] and for two laboratory experiments with chemical oscillators [panels (e)–(l)]. Panels (a), (e), and (i): Computed values of ζ_k (dots) and their semicircle fit (solid curve). Panels (b), (f), and (j): Approximated phase lag $\hat{\alpha}$ is the minimum of the function $P(\alpha)$, see formula (16). Panels (c), (g), and (k): The best fit (solid curve) of the dependence between Ω_k and $\hat{s}_k$ (dots). Panels (d), (h), and (l): Approximated $\hat{\omega}_k$ vs. actual ω_k natural frequencies. Reconstruction quality: (a) $C_1 = 0.002$ and (c) $C_2 = 0.999$, (e) $C_1 = 0.006$ and (g) $C_2 = 0.983$, and (i) $C_1 = 0.005$ and (k) $C_2 = 0.987$.

phase shift $\hat{\alpha} = 1.260$. This positive phase shift, which corresponds to the speeding up of the oscillations, was noted in the previous work [28] and has important consequence on the synchronization properties. For example, in this given partially synchronized population, all the unsynchronized cells have large natural frequencies. We note that the large phase shift could induce chimera states (e.g., coexistence of coherent and incoherent oscillations even without heterogeneities [29–31]) in network topologies of the circadian oscillator system.

The approximated coupling strength is $\hat{K} = 0.010$ and there is excellent correlation between the approximated and the actual natural frequencies, as shown in Fig. 9(d). We note that the two frequencies are not identical; instead, there is an offset of about 0.0090 rad/h. This offset exists because the shifted interaction function in the phase model (1) has nonzero value at zero phase difference. However, the coupling between the cells occurs through concentration differences; therefore, at zero phase difference the effect of coupling on the frequencies should be zero. The approximated natural frequencies $\hat{\omega}_k$ can be considered as dynamical frequencies, which have the same distribution as the original frequencies but could have an offset.

If we can assume that the coupling is through differences, then the offset can be approximated as $\hat{K} \sin \hat{\alpha} = 0.0095$ rad/h, which is in excellent agreement with the offset in the figure (0.009 rad/h).

The numerical simulations with the model thus predict that the universal relations could exist for the circadian gene expressions. Experimental implementation can use imaging of the circadian protein levels of the SCN slice cell population, e.g., using PER2-luciferase knock-in reporter [32]. The SCN cells have high levels of synchrony (close to phase-locked state) [32], nonetheless, as shown in Sec. IV C, even in this case a range of the phase lag parameter could be obtained that should reveal an important dynamical property of the circadian system.

B. Electrochemical oscillators

We test the existence of universal relations with the experimental data measured for a system of $N = 80$ chemical oscillatory units. The experimental systems consists of oscillatory nickel dissolution on a multielectrode array [15]. (See Appendix B for detailed description of the experimental

setup.) On the surface on each of the electrodes in the array, an oscillatory chemical reaction takes place (nickel electrodissolution). At constant circuit potential the rate of dissolution can be measured as the current, and the phases of the oscillations can be reconstructed with the Hilbert transform method [15]. Global coupling among the oscillators occurs when the electrodes are coupled to a potentiostat through a common (shunt) resistance. When the coupling is sufficiently strong, a partially synchronized states occur that was attributed to a Kuramoto transition by careful analysis of the order parameter as a function of coupling strength [15]. Now we use only a single data set to analyze the partially synchronized state. Figures 9(e)–9(h) show that complex parameters ζ_k and effective frequencies Ω_k (dots) do concentrate around the curves corresponding to universal relations predicted by the thermodynamic limit. This permits us to determine the values of all natural frequencies $\hat{\omega}_k$, see Fig. 9(h), as well as coupling strength $\hat{K} = 0.181$ and phase lag parameter $\hat{\alpha} = -0.009$. The nearly zero value of $\hat{\alpha}$ confirms the results of independent experiments that for coupling through resistance the phase shift parameter is nearly zero [33].

We also performed experiments in which a small capacitance was attached in parallel with the coupling resistance. In such scenario, the coupling signal cannot be described with difference of variables but instead occurs through a mediating dynamical variable (potential drop over the RC circuit). As shown in Figs. 9(i)–9(l), the universal relations still hold well and gave $\hat{K} = 0.115$ and a negative phase shift $\hat{\alpha} = -0.719$. The experiments thus confirm that the universal relations arise for complex coupling mechanism that can be effectively described with a phase lag in the interaction function.

Note that the phases of electrochemical oscillators above were obtained via the Hilbert transform of the corresponding current signals [15], and therefore the phases used in the parameter approximation algorithm not necessarily were physical phases of these oscillators. Although in our experiments we did not detect any loss of the parameter approximation accuracy, this can be different in other situations where the choice of unsuitable phase may result in uncontrolled systematic errors of the parameter approximation algorithm. In such cases, to avoid the problem one has to employ the protophase transformation [20,34,35].

VI. CONCLUSIONS

We showed that the local order parameter plot of a partially synchronized system exhibits universal features that can be interpreted with the Kuramoto-Sakaguchi model. The semicircle fit representation of the partially synchronized state is thus a promising diagnostic tool that can be used to investigate the dynamics of coupled oscillators. In particular, the noninvasive nature of the method makes it suitable for data obtained from living or engineered systems, where intervention (e.g., changing coupling strengths) could be costly or dangerous. The existence of the universal relations allows an initial approximation of coupling strength, phase-lag parameter, and the natural frequency of the oscillators. Similar techniques rely on fitting of the instantaneous frequencies to model equations [36,37]. The universal relations provide alternative means to such parameter reconstructions. An advantage of using our

parameter approximations is that they provide a simple visual representation through a semicircle fit, they rely on formulas containing time-averaged quantities, and the accuracy of the approximation improves for large system size. (With the fitting technique the accuracy typically decreases with increasing system size [36].) Moreover, the universal relations provided a range of self-consistency checks, e.g., for presence of network interactions and higher-order terms in the interaction functions. With full (instead of partial) synchronization, an upper and lower bound for the phase shift parameters can be defined, and a two-parametric set of approximated natural frequencies and coupling strengths can be calculated. If the experimental data are found to be consistent with the Kuramoto-Sakaguchi model, then a large array of techniques, based on phase model machinery, can be used for predictions and design of the system behavior, e.g., for desynchronization [4], optimal network architecture [38], or patterns induced by external entrainment [39]. Furthermore, the universal relations allow decomposition of extent of partially synchronized states in three contributing factors: (i) heterogeneity of natural frequencies, (ii) coupling strength, and (iii) coupling phase lag (e.g., delay). Such decomposition could greatly aid revealing the underpinning of collective behavior in large oscillator arrays, e.g., in densely connected brain regions responsible for generation of epileptic seizures [40].

We note that while the coupling among the oscillators was assumed global (all-to-all), this may not restrict the applications to situation where there is a physical link among every single node pairs in the network. A more common form of global coupling occurs through external constraints, where small change in one node dynamics is compensated globally to keep averaged quantity (e.g., temperature) constant. In fact, in the electrochemical experiments the potentiostat provided constant circuit potential (or driving force) for the reactions, which is a source of the global interactions.

In Sec. IV D we explained that universal relations (6)–(8) only allow us to judge whether a given system is of the Kuramoto-Sakaguchi type or not and, in the case of the positive answer, to estimate its parameters. But what can one do if the answer is negative? A possible way to avoid such situation is to develop the concept of universal relations for a more general class of phase oscillator models. For example, relations similar to (7) were reported for a Kuramoto-type model with distributed natural frequencies, coupling strengths, and phase lags [41–43]. Equipping them with analogs of formulas (6) and (8) one may hope to extend the applicability of universal relations at least in this particular direction. Other models, for which explicit universal relations can be derived using the Ott-Antonsen approach, include coupled theta-neurons [44] and the Winfree model [45]. Even for some Kuramoto models with nonsinusoidal phase interaction functions there is a chance to obtain explicit universal relations using the self-consistency analysis proposed in Ref. [46]. We plan to address some of these issues in our future work.

APPENDIX A: THERMODYNAMIC LIMIT THEORY FOR THE KURAMOTO MODEL

Phase reduction is a universal approach to reduce mathematical complexity of a system of nearly identical weakly coupled limit cycle oscillators independently of their nature. In the case of N globally (e.g., all-to-all) coupled oscillators it yields an N dimensional ODE system for phases $\theta_k \in \mathbb{R}$,

$$\frac{d\theta_k}{dt} = \omega_k - \frac{K}{N} \sum_{j=1}^{N} f(\theta_k - \theta_j), \quad k = 1, \dots, N, \quad \text{(A1)}$$

where $\omega_k \in \mathbb{R}$ are natural frequencies of the oscillators and $f : \mathbb{R} \to \mathbb{R}$ is a 2π-periodic interaction function.

In many practical cases one can assume that frequencies ω_k are drawn randomly from a specific distribution $g(\omega)$ and that function f is well approximated by the leading Fourier harmonics only, i.e., $f(\theta) = \sin(\theta + \alpha)$, where $\alpha \in (-\pi/2, \pi/2)$. Thus one obtains the Kuramoto-Sakaguchi model [8]

$$\frac{d\theta_k}{dt} = \omega_k - \frac{K}{N} \sum_{j=1}^{N} \sin(\theta_k - \theta_j + \alpha), \quad k = 1, \dots, N, \quad \text{(A2)}$$

which we discuss below.

In the limit $N \to \infty$ the state of the phase oscillators $\{\theta_k(t)\}$ in system (A2) can be described by a probability density function $\rho(\theta, \omega, t)$, which obeys the continuity equation

$$\frac{\partial \rho}{\partial t} + \frac{\partial}{\partial \theta}(\rho v) = 0, \quad \text{(A3)}$$

where

$$v(\theta, \omega, t) = \omega + \frac{K}{2i}[e^{-i\alpha} r(t) e^{-i\theta} - e^{i\alpha} \overline{r}(t) e^{i\theta}] \quad \text{(A4)}$$

is the continuum version of the velocity field in Eq. (A2), and

$$r(t) = \int_{-\infty}^{\infty} d\omega \int_{0}^{2\pi} \rho(\omega, \theta, t) e^{i\theta} d\theta \quad \text{(A5)}$$

is the Kuramoto order parameter [47]. Moreover, for any complex variable a we use $\overline{a}$ to denote its complex conjugate.

It is well known [25] that long-time dynamics of solutions to Eq. (A3) have tendency to settle down at the so-called Ott-Antonsen manifold consisting of the distributions of the form

$$\rho(\theta, \omega, t) = \frac{g(\omega)}{2\pi} \left\{ 1 + \sum_{n=1}^{\infty} [\overline{z}^n(\omega, t) e^{in\theta} + z^n(\omega, t) e^{-in\theta}] \right\}, \quad \text{(A6)}$$

where $z(\omega, t)$ satisfies the inequality $|z| \leqslant 1$ and solves the differential equation

$$\frac{dz}{dt} = i\omega z(\omega, t) + \frac{K}{2} e^{-i\alpha} \mathcal{G} z - \frac{K}{2} e^{i\alpha} z^2(\omega, t) \mathcal{G} \overline{z} \quad \text{(A7)}$$

with $\mathcal{G} z$ denoting the integral operator

$$(\mathcal{G} z)(t) = \int_{-\infty}^{\infty} g(\omega) z(\omega, t) d\omega. \quad \text{(A8)}$$

From (A6) it follows that

$$z(\omega, t) = \int_{0}^{2\pi} \frac{\rho(\theta, \omega, t)}{g(\omega)} e^{i\theta} d\theta. \quad \text{(A9)}$$

For coupled oscillator system (A2) the integral in the right-hand side of (A9) is approximately equivalent to the sum

$$\frac{1}{\#\{k \ : \ \omega_k \approx \omega\}} \sum_{k \ : \omega_k \approx \omega} e^{i\theta_k}$$

that resembles the definition of the Kuramoto order parameter (2) with summation carried out over oscillators with $\omega_k \approx \omega$ only. This means that function $z(\omega, t)$ is a local synchrony characteristics with values depending on natural frequencies ω, and therefore we call it the local order parameter.

Considering Eq. (A7) one usually is interested in the existence and stability of the following two types of solutions: (i) completely incoherent state $z(\omega, t) = 0$ and (ii) partially synchronized states:

$$z(\omega, t) = a(\omega) e^{i\Omega t}, \quad \text{(A10)}$$

where for different values of $\omega \in \operatorname{supp} g$ one has either $|a(\omega)| = 1$ (coherence) or $|a(\omega)| < 1$ (incoherence).

In Refs. [21,22] it has been shown that independent of the choice of distribution $g(\omega)$, the amplitude $a(\omega)$ of a stable partially synchronized state is always given by the formula

$$a(\omega) = h\left(\frac{\omega - \Omega}{p}\right), \quad \text{(A11)}$$

where

$$h(s) = \begin{cases} (1 - \sqrt{1 - s^{-2}})s & \text{for} \quad |s| > 1 \\ s - i\sqrt{1 - s^2} & \text{for} \quad |s| \leqslant 1 \end{cases},$$

is a universal function and $(\Omega, p) \in \mathbb{R} \times (0, \infty)$ is a pair of numbers satisfying the self-consistency equation

$$\frac{1}{K} e^{i\alpha} = \frac{i}{p} \int_{-\infty}^{\infty} g(\omega) h\left(\frac{\omega - \Omega}{p}\right) d\omega. \quad \text{(A12)}$$

In other words, stationary partially synchronized solutions of Eq. (A3) constitute a two-parametric family with explicitly known distribution $\rho(\theta, \omega, t)$. The latter is obtained if we insert (A10) and (A11) into (A6).

Using this distribution we can compute various averaged quantities. For example, inserting $\rho(\theta, \omega, t)$ into (A5) and taking into account the self-consistency equation (A12) we obtain

$$r(t) = -\frac{p}{K} i e^{i\alpha} e^{i\Omega t}$$

and hence

$$|r(t)| = p/K. \quad \text{(A13)}$$

Next we can calculate the mean phase velocity of the oscillators with natural frequencies $\omega_k \approx \omega$. This will be

$$\frac{1}{\#\{k \ : \ \omega_k \approx \omega\}} \sum_{k \ : \omega_k \approx \omega} v(\theta_k, \omega_k, t).$$

For a given distribution $\rho(\theta, \omega, t)$ we can replace the latter averaging with the formula

$$\int_{0}^{2\pi} \frac{\rho(\theta, \omega, t)}{g(\omega)} v(\theta, \omega, t) d\theta.$$

Note that since we take into account only oscillators with $\omega_k \approx \omega$, we average only over the phase variable θ and use in the integrand conditional probability distribution $\rho(\theta,\omega,t)/g(\omega)$ instead of the bivariate distribution $\rho(\theta,\omega,t)$. Omitting computation details, which can be found in Ref. [22, Section 3.3], in the result we obtain

$$\Psi(\omega) = \int_0^{2\pi} \frac{\rho(\theta,\omega,t)}{g(\omega)} v(\theta,\omega,t) d\theta$$
$$= \omega - \mathrm{Re}\left[p\, h\left(\frac{\omega-\Omega}{p}\right) \right]$$
$$= \Omega + p\, Q\left(\frac{\omega-\Omega}{p}\right), \qquad (A14)$$

where

$$Q(s) = \begin{cases} s\sqrt{1-s^{-2}} & \text{for} \quad |s| > 1, \\ 0 & \text{for} \quad |s| \leqslant 1 \end{cases}$$

is another universal function.

Similarly, for every positive integer n we can calculate another quantity

$$\zeta^{(n)}(\omega) = \frac{1}{\#\{k\,:\,\omega_k \approx \omega\}} \sum_{k\,:\,\omega_k \approx \omega} (-i)^n e^{in\theta_k(t)} \frac{\overline{r}(t)^n}{|r(t)|^n},$$

which is relevant to the amplitude $a(\omega)$ of the local order parameter (A10). Indeed, by analogy with the mean phase velocity we obtain

$$\zeta^{(n)}(\omega) = \int_0^{2\pi} \frac{\rho(\theta,\omega,t)}{g(\omega)} (-i)^n e^{in\theta} \frac{\overline{r}(t)^n}{|r(t)|^n} d\theta$$
$$= \left[h\left(\frac{\omega-\Omega}{p}\right) e^{-i\alpha} \right]^n, \qquad (A15)$$

hence $\zeta^{(n)}(\omega) = (a(\omega)e^{-i\alpha})^n$.

Numerical simulations suggest that in the thermodynamic limit $N \to \infty$ partially synchronized states of Eq. (A2) have the ergodicity property such that ensemble averages (A14) and (A15) can be calculated as time averages for fixed choice of ω. Therefore we obtain

$$\Psi(\omega_k) = \omega_k - \mathrm{Re}\left[p\, h\left(\frac{\omega_k-\Omega}{p}\right) \right]$$
$$= \Omega + p\, Q\left(\frac{\omega_k-\Omega}{p}\right), \qquad (A16)$$

$$\zeta^{(n)}(\omega_k) = \left[h\left(\frac{\omega_k-\Omega}{p}\right) e^{-i\alpha} \right]^n. \qquad (A17)$$

Moreover, if R denotes the time-average of $|r(t)|$, then according to (A13) we should have

$$R = p/K. \qquad (A18)$$

Combining formulas (A16)–(A18) we also obtain other relations. For example, formula (A17) implies

$$\zeta^{(n)}(\omega_k) = [\zeta^{(1)}(\omega_k)]^n. \qquad (A19)$$

Furthermore, expressing p from (A18) and $h[(\omega_k-\Omega)/p]$ from (A17) and inserting them into (A16) we obtain

$$\Psi(\omega_k) = \omega_k - K R\, \mathrm{Re}\left[\zeta^{(1)}(\omega_k) e^{i\alpha} \right]. \qquad (A20)$$

Formulas (A16)–(A20) are exact for $N \to \infty$ only; however, they seem to be a good approximation for large but fixed N, too. Their accuracy is studied in the main text of the paper. There we also discuss some of their practical applications.

APPENDIX B: EXPERIMENTAL SETUP

A standard three electrode electrochemical cell is used for the experiments where the reference electrode is Hg/Hg$_2$SO$_4$/sat. K$_2$SO$_4$, the counterelectrode, is a platinum-coated titanium rod, and the working electrode is an array of 80 nickel wires embedded in epoxy such that only the 1.00-mm diameter surface is exposed to the 3 M H$_2$SO$_4$ electrolyte (see Fig. 10). The temperature is held at 10°C with a circulating bath.

A constant circuit potential ($V = 1120$ mV) is applied with a potentiostat (ACM Instruments GillAC), and the smooth current oscillations are collected at a rate of 200 Hz.

Each nickel electrode is connected to the potentiostat through the collective (R_{col}) and individual resistances (R_{ind}) as shown in Fig. 10. The collective (shunt) resistance introduces global coupling among the electrode potentials of the electrodes [15]. With $R_{\mathrm{col}} = 0.5$ Ohm and $R_{\mathrm{ind}} = 1$ kOhm a partially synchronized state was observed in the experiments.

Nonisochronicity is introduced into the system by the addition of capacitance parallel to both resistances; collective capacitance (C_{col}) and individual capacitance (C_{ind}). The level of nonisochronicity induced by the capacitance was studied previously [33]. In the experiments with phase shift in the interaction function, $C_{\mathrm{col}} = 1.1$ mF and $C_{\mathrm{ind}} = 220$ μF were applied.
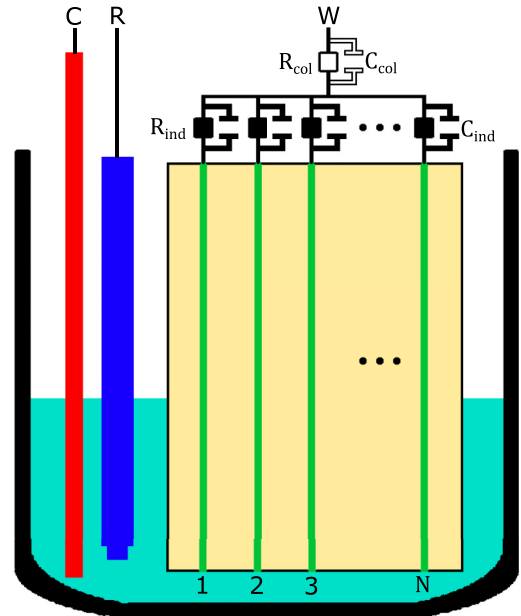
FIG. 10. Diagram of the experimental setup. C: Counterelectrode; R: reference electrode; W: working electrode. The individual resistances and capacitances are filled while the collective resistance and capacitance are hollow.

[1] A. Pikovsky, M. Rosenblum, and J. Kurths, *Synchronization, A Universal Concept in Nonlinear Sciences* (Cambridge University Press, Cambridge, 2001).

[2] A. Winfree, *The Geometry of Biological Time* (Springer, Berlin, 2001).

[3] F. C. Hoppensteadt and E. M. Izhikevich, *Weakly Connected Neural Networks* (Springer, Berlin, 1997).

[4] P. A. Tass, *Phase Resetting in Medicine and Biology* (Springer, Berlin, 1999).

[5] L. Glass, Nature **410**, 277 (2001).

[6] J. Jalife, J. Physiol. **356**, 221 (1984).

[7] S. Yamaguchi, H. Isejima, T. Matsuo, R. Okura, K. Yagita, M. Kobayashi, and H. Okamura, Science **302**, 1408 (2003).

[8] H. Sakaguchi and Y. Kuramoto, Prog. Theor. Phys. **76**, 576 (1986).

[9] A. Pikovsky and M. Rosenblum, Chaos **25**, 097616 (2015).

[10] K. Wiesenfeld, P. Colet, and S. H. Strogatz, Phys. Rev. Lett. **76**, 404 (1996).

[11] K. Wiesenfeld, P. Colet, and S. H. Strogatz, Phys. Rev. E **57**, 1563 (1998).

[12] A. A. Temirbayev, Z. Zh. Zhanabaev, S. B. Tarasov, V. I. Ponomarenko, and M. Rosenblum, Phys. Rev. E **85**, 015204 (2012).

[13] L. Q. English, Z. Zeng, and D. Mertens, Phys. Rev. E **92**, 052912 (2015).

[14] L. Q. English, D. Mertens, S. Abdoulkary, C. B. Fritz, K. Skowronski, and P. G. Kevrekidis, Phys. Rev. E **94**, 062212 (2016).

[15] I. Z. Kiss, Y. Zhai, and J. L. Hudson, Science **296**, 1676 (2002).

[16] J. Garcia-Ojalvo, M. B. Elowitz, and S. H. Strogatz, Proc. Natl. Acad. Sci. USA **101**, 10955 (2004).

[17] S. D. Monte, F. d'Ovidio, S. Danø, and P. G. Sørensen, Proc. Natl. Acad. Sci. USA **104**, 18377 (2007).

[18] A. F. Taylor, M. R. Tinsley, F. Wang, Z. Huang, and K. Showalter, Science **323**, 614 (2009).

[19] A. Weber, Y. Prokazov, W. Zuschratter, and M. J. B. Hauser, PLoS ONE **7**, e43276 (2012).

[20] B. Kralemann, L. Cimponeriu, M. Rosenblum, A. Pikovsky, and R. Mrowka, Phys. Rev. E **77**, 066205 (2008).

[21] O. E. Omel'chenko and M. Wolfrum, Phys. Rev. Lett. **109**, 164101 (2012).

[22] O. E. Omel'chenko and M. Wolfrum, Physica D (Amsterdam) **263**, 74 (2013).

[23] S. H. Strogatz, Physica D (Amsterdam) **143**, 1 (2000).

[24] J. A. Acerbrón, L. L. Bonilla, C. J. Pérez-Vicente, F. Ritort, and R. Spigler, Rev. Mod. Phys. **77**, 137 (2005).

[25] E. Ott and T. M. Antonsen, Chaos **18**, 037113 (2008).

[26] E. Ott and T. M. Antonsen, Chaos **19**, 023117 (2009).

[27] J.-C. Leloup and A. Goldbeter, Proc. Natl. Acad. Sci. USA **100**, 7051 (2003).

[28] S. Schroder, E. D. Herzog, and I. Z. Kiss, J. Biol. Rhythms **27**, 79 (2012).

[29] D. M. Abrams and S. H. Strogatz, Phys. Rev. Lett. **93**, 174102 (2004).

[30] M. J. Panaggio and D. M. Abrams, Nonlinearity **28**, R67 (2015).

[31] O. E. Omel'chenko, Nonlinearity **31**, R121 (2018).

[32] E. D. Herzog, I. Z. Kiss, and C. Mazuski, Methods Enzymol. **552**, 3 (2015).

[33] M. Wickramasinghe and I. Z. Kiss, Phys. Rev. E **88**, 062911 (2013).

[34] B. Kralemann, M. Frühwirth, A. Pikovsky, M. Rosenblum, T. Kenner, J. Schaefer, and M. Moser, Nat. Commun. **4**, 2418 (2013).

[35] B. Kralemann, A. Pikovsky, and M. Rosenblum, New J. Phys. **16**, 085013 (2014).

[36] I. T. Tokuda, S. Jain, I. Z. Kiss, and J. L. Hudson, Phys. Rev. Lett. **99**, 064101 (2007).

[37] A. Pikovsky, Phys. Lett. A **382**, 147 (2018).

[38] P. S. Skardal, D. Taylor, and J. Sun, Phys. Rev. Lett. **113**, 144101 (2014).

[39] A. Zlotnik, R. Nagao, I. Z. Kiss, and J.-S. Li, Nat. Commun. **7**, 10788 (2016).

[40] M. Sadilek and S. Thurner, Sci. Rep. **5**, 10015 (2015).

[41] D. Iatsenko, P. V. E. McClintock, and A. Stefanovska, Nat. Commun. **5**, 4118 (2014).

[42] D. Iatsenko, S. Petkoski, P. V. E. McClintock, and A. Stefanovska, Phys. Rev. Lett. **110**, 064101 (2013).

[43] S. Petkoski, D. Iatsenko, L. Basnarkov, and A. Stefanovska, Phys. Rev. E **87**, 032908 (2013).

[44] T. B. Luke, E. Barreto, and P. So, Neural Comput. **25**, 3207 (2013).

[45] R. Gallego, E. Montbrió, and D. Pazó, Phys. Rev. E **96**, 042208 (2017).

[46] M. Komarov and A. Pikovsky, Phys. Rev. Lett. **111**, 204101 (2013).

[47] J. D. Crawford and K. T. R. Davies, Physica D (Amsterdam) **125**, 1 (1999).

[48] E. A. Martens, E. Barreto, S. H. Strogatz, E. Ott, P. So, and T. M. Antonsen, Phys. Rev. E **79**, 026204 (2009).

[49] E. Montbrió, J. Kurths, and B. Blasius, Phys. Rev. E **70**, 056125 (2004).

[50] For a stationary partially synchronized state, dynamics of system (1) does not display any macroscopic oscillations beyond finite-size fluctuations, which, in particular, are visible in the time trace of $|r(t)|$. Nonstationary partially synchronized regimes also can be found in system (1) although less frequently. Their examples were reported for bimodal distributions of natural frequencies [48] as well as for two-population models [49].